https://doi.org/10.3311/PPci.40462

Periodica Polytechnica Civil Engineering, 69(3), pp. 999–1018, 2025

Effect of Local Shear Deformation and Soil Flexibility on the Global Buckling Stability of Uniform and Non-uniform Buildings

Mao Cristian Pinto-Cruz[1,2*]

[1] Department of Civil and Environmental Engineering, Pontifical Catholic University of Rio de Janeiro, Rua Marquês de São Vicente 225., 22451-900 Rio de Janeiro, Brazil
[2] Department of Civil Engineering, National University of Engineering, Avenue Túpac Amaru 210., 15333 Lima, Peru
[*] Corresponding author, e-mail: maopintouni@gmail.com

Received: 17 March 2025, Accepted: 08 July 2025, Published online: 30 July 2025

Abstract

Traditional continuous models do not capture the deformation mechanism due to local shear in coupled shear wall-based buildings, resulting in a significant underestimation of the global buckling loads. To address this limitation, the present study introduces a novel generalized sandwich-type continuous beam to derive both analytical and numerical solutions for estimating the global critical buckling load in buildings with uniform and non-uniform properties. A closed-form analytical solution is developed for uniform buildings subjected to a top-concentrated axial load, while a numerical approach – based on a modified transfer matrix method – accommodates arbitrarily distributed vertical loads and variable stiffness distributions. Soil flexibility is incorporated by modeling lateral and rotational springs at the base. The proposed numerical method maintains a constant matrix size (6 × 6), regardless of the number of discretized segments, with coefficients derived analytically. Validation against finite element models shows excellent agreement. A parametric study involving 954 cases indicates that the proposed continuous beam and its solution method limits the maximum error to –4.40%, lying on the conservative (safe) side of structural design. In contrast, the classical continuous beam shows errors up to –144.71%, raising concerns over its reliability. Furthermore, soil flexibility was found to reduce the critical buckling load by as much as 46.09%. The results underscore the robustness and practical applicability of the proposed continuous beam and its solution methods, providing a reliable framework for the structural analysis and design of buildings with coupled shear walls.

Keywords

wall deformation, generalized sandwich-type continuous beam, critical load, global stability analysis, building, soil-structure interaction

1 Introduction

The determination of the global critical buckling load in tall buildings is fundamental for assessing overall structural performance, particularly as structural slenderness increases. However, there remains a lack of comprehensive research focused on developing a unified analytical and numerical framework capable of evaluating tall buildings with varying geometric, structural, and material properties along their height, especially under complex vertical loading scenarios. It is well established that variable boundary conditions and nonuniform vertical load profiles hinder the derivation of closed-form analytical solutions [1]. Moreover, as the length of shear walls in lateral load-resisting systems increases, a new rotational field emerges, associated with the local shear behavior of these walls. Classical continuous models, frequently adopted in structural engineering, typically neglect this effect, leading to considerable discrepancies when compared to the accurate results obtained from advanced commercial finite element software.

There is a broad consensus in the current literature regarding the inherent complexity of formulating differential equations with variable coefficients for the global stability analysis of continuous beams, whether uniform or non-uniform, which often prevents the derivation of closed-form analytical solutions. A widely accepted and computationally efficient alternative is the classical transfer matrix method, which allows internal displacements and forces at any point along the continuous beam to be expressed in terms of those at the base of the coordinate system. This effectively transforms boundary value problems into initial value problems. However, a significant limitation of the classical transfer matrix method lies in

Cite this article as: Pinto-Cruz, M. C. "Effect of Local Shear Deformation and Soil Flexibility on the Global Buckling Stability of Uniform and Non-uniform Buildings", Periodica Polytechnica Civil Engineering, 69(3), pp. 999–1018, 2025. https://doi.org/10.3311/PPci.40462

its dependence on the computation of the inverse of the zero-transfer matrix, which leads to substantial computational costs. These costs increase with both the size of the matrix and the number of discretized segments along the continuous beam.

This study addresses these limitations by introducing a novel generalized sandwich-type continuous beam, along with a modified version of the classical transfer matrix method. Specifically developed to capture the deformation mechanism due to the local shear behavior of shear walls, the enhanced model is accompanied by a comprehensive solution strategy capable of analyzing buildings with geometric and mechanical properties that vary continuously or piecewise along their height, under arbitrary vertical loading conditions. Furthermore, the methodology incorporates soil flexibility through a simplified representation of soil–structure interaction, thereby extending its applicability to real-world structural engineering problems.

Although the development of finite element software packages is currently well established, it is useful to develop analytical, semi-analytical and numerical solutions that allow postgraduate students, academics and professionals to better understand the types of behavior of buildings with particular characteristics. The continuous method and the transfer matrix method are simple tools to implement at a low computational cost and have been used in various research related to building analysis. The initial application of a continuous beam to analyze building behavior is credited to Chitty and Wan [2, 3]. They investigated the static characteristics of tall buildings using a uniform continuous beam that combined a bending beam and a shear beam in parallel. Despite simplifications and the omission of axial deformation in vertical elements, their work played a pivotal role in introducing continuous beams to the structural analysis of tall buildings. Potzta and Kollár [4], based on an energy balance of the potential deformation energy of the classic sandwich beam of the equivalent model and the structural elements, determined the bending and shear stiffness of the equivalent sandwich beam. Aksogan et al. [5–8] proposed a general closed-form analytical method for the dynamic analysis of coupled shear walls with arbitrary sections. Zalka [9–11], using the continuous method and the classic continuous sandwich beam, proposed various comprehensive solutions for the static, dynamic and stability study of buildings. Xu and Li [12] deduced calculation formulas for the lateral displacement of shear walls coupled with cavities subjected to three different lateral loading scenarios. Hu et al. [13] presented a generalized method to estimate the drifts of tall buildings composed of flat moment frames and coupled shear walls. In his model, he introduced the axial deformations of the columns and walls, the bending and shear deformations of the beams, the double curvature bending and shear deformations of the columns or walls and incorporated the P-Delta effects into the stiffness matrix. Tong and Lin [14] introducing a simplified model, determined the relationships between the buckling and vibration characteristics of coupled shear walls with various parameters and defined an upper limit of periods as a practical tool to manage second-order effects. Wang et al. [15] using the displacement method derived analytical solutions for the static analysis of shear walls subjected to three different cases of lateral loading. Zhang et al. [16] proposed analytical solutions to determine the additional axial forces and coupling ratio of coupled shear walls.

However, these studies did not consider the local shear stiffness of the walls. The results of the parametric analysis conducted in this study, based on the classical sandwich beam model reported in the literature, revealed alarming error ranges when this effect is neglected – all on the side of structural unconservatism. Therefore, recently, efforts have been dedicated to introduce this behavior in the formulations of continuous beams using the continuous method, the discrete periodic media homogenization method and the transfer matrix method. Chesnais et al. [17, 18] were the first to rigorously study this behavior. Using the homogenization method of discrete periodic media, they carried out a complete study of the dynamic behavior, established the justifying hypotheses of the proposed model and derived closed-form analytical solutions for the dynamic study of buildings. Bozdogan et al. [19–25] using the continuous model of two Timoshenko beams coupled in parallel, proposed numerical solutions for the analysis of coupled shear walls and wall-frame buildings. The proposed solution method is simple and easy to implement computationally. Xia et al. [26] proposed an efficient method that takes into account the shear deformation of the shear wall and the restrained moment of the tie beam to perform preliminary analyzes of wall-frame buildings with vertically varying properties. Recently, the author of the present article continued the work of Chesnais et al. [17, 18], formally introducing a novel generalized sandwich-type continuous beam and deriving its corresponding solution methods for static [27–28], dynamic [29], and stability analyses [30]. For the static analysis, an analytical solution was proposed

for both uniform and non-uniform buildings subjected to lateral loads with a general distribution profile [27], along with a closed-form analytical solution for uniform buildings, in which the lateral displacement was decomposed into its three distinctive components: bending, shear, and interaction [28]. For the dynamic analysis, both analytical and numerical solutions were developed, incorporating soil flexibility and rotational inertias [29]. Finally, for the global stability analysis, analytical and semi-analytical solutions were presented for uniform buildings under vertically distributed loads with general profiles [30].

Therefore, by employing generalized sandwich-type continuous beam, presented by Pinto [27–30], this study addresses four outstanding challenges in the global stability analysis of buildings:

1. incorporating the deformation mechanism associated with the local shear behavior of walls into the classical formulation,
2. proposing analytical and numerical methods for calculating the global critical buckling load of buildings with uniform and/or non-uniform properties subjected to arbitrarily distributed vertical loads,
3. investigating the combined effects of wall shear deformation and soil flexibility on the estimation of the global critical buckling load; and,
4. extending the applicability of continuous models while enhancing their accuracy and predictive capability.

The outline of this paper is as follows. Section 2 presents the proposed continuous beam and the model assumptions. Section 3 shows the calculation of the equivalent rigidities of the continuous model. Section 4 presents the derivation of the equilibrium equations. Section 5 presents the proposed numerical solution. Section 6 analyzes the particular case that allows obtaining a closed-form analytical solution, Section 7 details the computational implementation procedure, Section 8 presents the numerical applications and Section 9 presents the conclusions of the research.

2 Proposed continuous model

The author recently introduced the concept of the generalized sandwich-type continuous beam (hereinafter referred to as the generalized sandwich beam) in a prior publication focused on the comprehensive analysis of buildings with extended shear walls [27–30]. Broadly, the generalized sandwich beam is characterized by four stiffness parameters and three kinematic fields, providing a thorough representation of all conceivable behaviors exhibited by buildings. The incorporation of local shear stiffness in the mathematical formulation enables the consideration of four fundamental modes of deformation: global shear (Fig. 1 (a)), global bending (Fig. 1 (b)), local bending (Fig. 1 (c)), and local shear (Fig. 1 (d)).

The generalized sandwich beam results from the series coupling of a classical sandwich beam and a shear beam, where the sandwich beam itself is formed by the parallel coupling of a Timoshenko beam and a bending beam. The generalized sandwich beam introduces an additional kinematic field of rotation, enabling the inclusion of local shear deformation typically observed in stiffer elements such as shear walls. This enhancement, together with the explicit consideration of shear stiffness, renders the generalized sandwich beam a suitable replacement model for analyzing buildings with significant shear wall components. Mathematically, the equivalent column (Fig. 2) is characterized by four stiffness parameters: k_{b1}, k_{s1}, k_{b2}, and k_{s2} corresponding to global bending stiffness, global

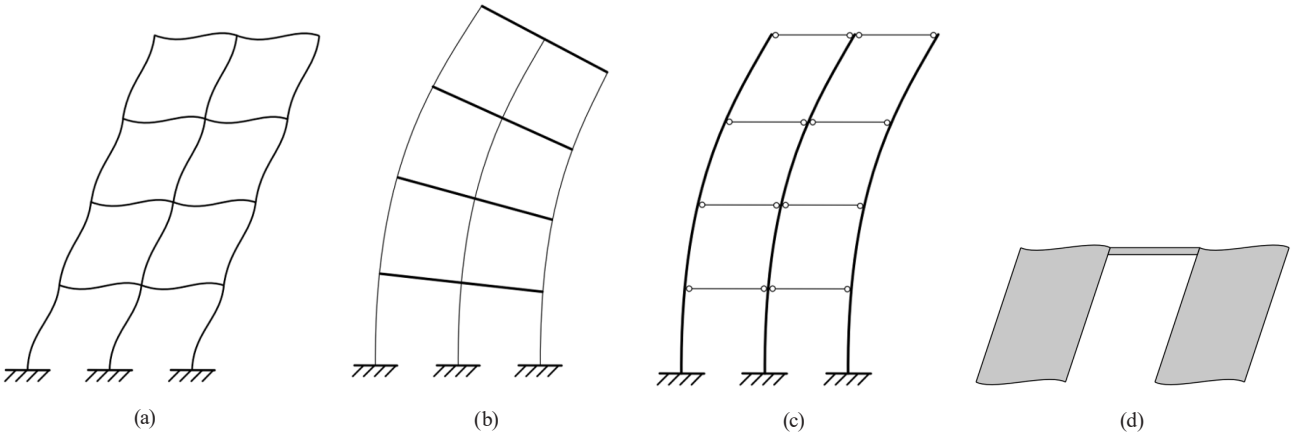

Fig. 1 Deformation mechanism [11] a) Global shear K_{s1}, b) global bending K_{b1}, c) local bending K_{b2}, and, d) local shear K_{s2}

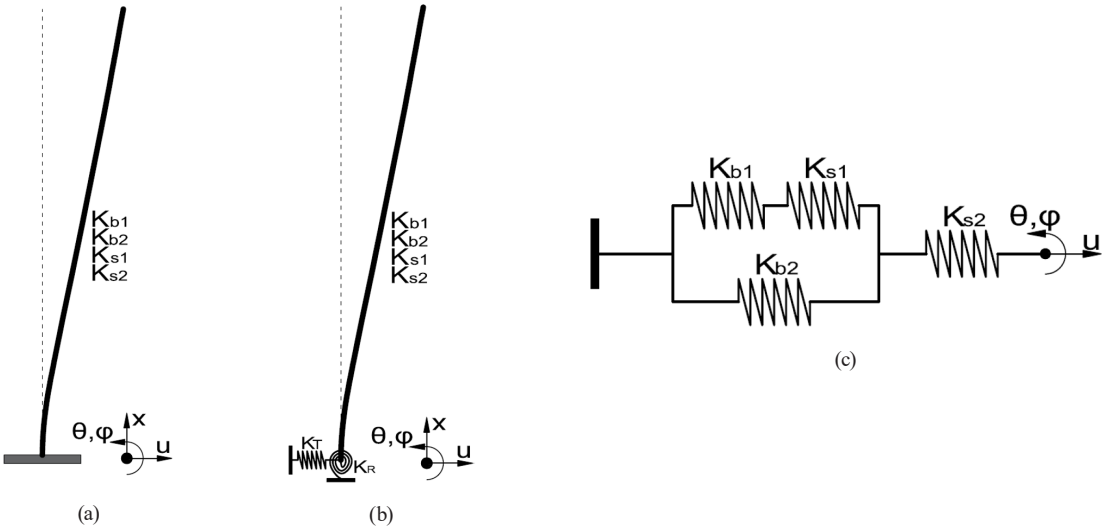

Fig. 2 Generalized sandwich beam a) Equivalent column with fixed base, b) Equivalent column with flexible base, and, c) Association of mechanisms

shear stiffness, local bending stiffness, and local shear stiffness, respectively, and three kinematic fields: one lateral displacement field u, and two rotational fields due to global bending θ and local bending φ. Figs. 2 (a)–(c) illustrate the mechanical idealization, the incorporation of soil flexibility into the continuous model for evaluating global buckling loads, and the coupling mechanisms of deformation within the proposed formulation.

The proposed continuous formulation and the corresponding solution method are restricted by the following assumptions:

1. the material behavior is linear-elastic and adheres to small-displacement theory,
2. the discrete shear forces in the coupling beams are replaced by an equivalent continuous shear flow,
3. the walls are subjected to in-plane stress and are assumed to have rigid cross-sections,
4. the coupling beams are axially inextensible,
5. identical rotational fields are assumed for all walls, and,
6. both the coupling beams and walls are modeled as Timoshenko beams, with strain energy arising from both bending and shear deformations.

Although the continuous model does not impose a strict lower limit on the number of stories in a coupled shear wall system, maintaining the validity of the homogenization hypothesis and achieving acceptable accuracy in predicting lateral displacements requires a minimum of five stories.

3 Equivalent stiffness of the proposed continuous model

The equivalent stiffnesses of the continuous model for a building whose lateral bracing system is based on coupled shear walls can be calculated using the equations established in the literature [11], which are rewritten below.

The bending stiffness of the beam assembly is calculated as:

$$K_b = \sum \frac{6EI_b\left(\left(1^* + s_1\right)^2 + \left(1^* + s_2\right)^2\right)}{1^{*3}h\left(1 + 12\dfrac{EI_b}{1^{*2}GA_b^{'}}\right)}, \tag{1}$$

where E is the modulus of elasticity of the structure, G is the shear modulus of the structure, I_b is the second moment of area of the beams, $A_b^{'}$ is the cross-sectional area of the beams reduced by a factor of 0.83 due to the shear effect, l^* is the distance between the two wall sections, s_1 and s_2 are the lengths of the wall sections of the coupled shear walls, and h is the storey height.

- The bending stiffness of the coupled shear walls is calculated as:

$$K_w = \sum \frac{\pi^2 EI_w}{h^2}, \tag{2}$$

where I_w is the second moment of area of the walls. The reduction factor for local bending stiffness is calculated as:

$$r = \frac{K_w}{K_w + K_b}. \tag{3}$$

- The global bending stiffness is calculated as:

$$K_{bl} = E\sum A_w l^2, \tag{4}$$

where A_w *s* the cross-sectional area of the walls and *l* is the length between the centroid of the wall and the centroid of the total walls.

- The global shear stiffness is calculated as:

$$K_{s1} = \frac{K_b K_w}{K_b + K_w}. \tag{5}$$

- Local bending stiffness is calculated as:

$$K_{b2} = rE\sum I_w. \tag{6}$$

- The local shear stiffness is calculated as:

$$K_{s2} = G\sum A_w^{'}, \tag{7}$$

where $A_w^{'}$ is the cross-sectional area of the walls reduced by a factor of 0.83 due to the shear effect.

For buildings with arbitrary horizontal bracing systems, comprising a combination of independent structural subsystems such as frames, coupled shear walls, and cores, a more general analysis strategy is required. The reader is referred to Section 2.2 of [31] for further details.

4 Derivation of equilibrium equations

The strain energy of the generalized sandwich beam, taking into account the soil flexibility, is formulated as follows:

$$V = \frac{1}{2}\int_0^H \left\{K_{b1}\theta^{'2}(x) + K_{s1}\left[\theta(x) - \varphi(x)\right]^2 + K_{b2}\varphi^{'2}(x) + K_{s2}\left[\varphi(x) - u^{'}(x)\right]^2\right\}dx + \frac{1}{2}K_T u^2(0) + \frac{1}{2}K_R\theta^2(0). \tag{8}$$

where, the expressions $\frac{1}{2}\int K_{b1}\theta^{'2}(x)dx$, $\frac{1}{2}\int K_{s1}\left[\theta(x) - \varphi(x)\right]^2 dx$, $\frac{1}{2}\int K_{b2}\varphi^{'2}(x)dx$ and $\frac{1}{2}\int K_{s2}\left[\varphi(x) - u'(x)\right]^2 dx$ represent the contributions to potential energy arising from global bending, local shear, local bending, and local shear, respectively. The introduction of soil flexibility is characterized by translational and rotational springs, denoted as K_T and K_R, respectively.

In examining the critical load associated with global buckling, an analysis is conducted considering a vertically distributed load along the height of the building (Fig. 3). The work done by the arbitrary vertical load (Fig. 3) is denoted as [32]:

$$W = \frac{1}{2}\int_0^H P(x)u^{'2}(x)dx. \tag{9}$$

The Lagrangian functional, is formulated as:

$$\Pi = \frac{1}{2}\int_0^H \left\{K_{b1}\theta^{'2}(x) + K_{s1}\left[\theta(x) - \varphi(x)\right]^2 + K_{b2}\varphi^{'2}(x) + K_{s2}\left[\varphi(x) - u^{'}(x)\right]^2\right\}dx + \frac{1}{2}K_T u^2(0) + \frac{1}{2}K_R\theta^2(0) - \frac{1}{2}\int_0^H P(x)u^{'2}(x)dx. \tag{10}$$

The resolution of this Lagrangian functional is accomplished through the application of Hamilton's principle.

$$\delta\int_{t1}^{t2}(V - W)dt = \delta\int_{t1}^{t2} Udt = 0. \tag{11}$$

In other words:

$$\begin{aligned}
\delta\Pi = &\int_0^H \left\{-\left[K_{s2} - P(x)\right]u^{''}(x) + K_{s2}\varphi^{'}(x)\right\}\delta u(x)dx + \int_0^H \left\{-K_{b1}\theta^{''}(x) + K_{s1}\left[\theta(x) - \varphi(x)\right]\right\}\delta\theta(x)dx \\
&+\int_0^H \left[-K_{b2}\varphi^{''}(x) + (K_{s1} + K_{s2})\varphi(x) - K_{s1}\theta(x) - K_{s2}u^{'}(x)\right]\delta\varphi(x)dx \\
&+\left\{\left[K_{s2} - P(x)\right]u^{'}(x) - K_{s2}\varphi(x)\right\}\delta u(x)\Big|_0^H + \left[K_{b1}\theta^{'}(x)\right]\delta\theta(x)\Big|_0^H + \left[K_{b2}\varphi^{'}(x)\right]\delta\varphi(x)\Big|_0^H \\
&+K_T u(0)\delta u(0) + K_R\theta(0)\delta\theta(0) = 0.
\end{aligned} \tag{12}$$

The constitutive laws are defined as:

$$M_1(x) = K_{bl}\theta^{'}(x), \tag{13}$$

$$M_2(x) = K_{b2}\varphi^{'}(x), \tag{14}$$

$$V(x) = \left[K_{s2} - P(x)\right]u^{'}(x) - K_{s2}\varphi(x). \tag{15}$$

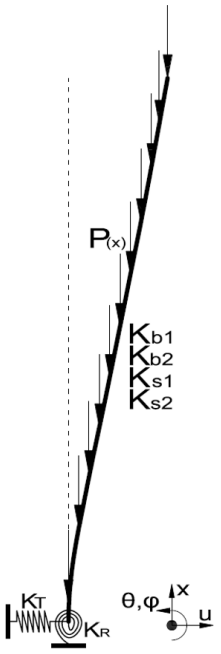

Fig. 3 Application of the vertical distributed load along the length of the proposed continuous model. *Note: P(x), as a real distributed load, is modeled as a sequence of equivalent point loads P, acting at the story levels of the structure*

Solving the set of differential equations resulting from stationarity yields a system of three equilibrium equations.

$$\delta u(x): -\left[K_{s2} - P(x)\right]u''(x) + K_{s2}\varphi'(x) = 0, \tag{16}$$

$$\delta\theta(x): -K_{b1}\theta''(x) + K_{s1}\left[\theta(x) - \varphi(x)\right] = 0, \tag{17}$$

$$\begin{aligned}\delta\varphi(x): &-K_{b2}\varphi''(x) + (K_{s1} + K_{s2})\varphi(x) - K_{s1}\theta(x)\\ &-K_{s2}u'(x) = 0.\end{aligned} \tag{18}$$

The boundary conditions associated with the flexible basis model are written below.

At the bottom of the model:

$$u(0) = \frac{V(0)}{K_T}, \tag{19}$$

$$\theta(0) = \frac{M_1(0)}{K_R}, \tag{20}$$

$$\varphi(0) = 0. \tag{21}$$

At the top of the model:

$$M_1(H) = K_{b1}\theta'(H) = 0, \tag{22}$$

$$M_2(H) = K_{b2}\varphi'(H) = 0, \tag{23}$$

$$V(H) = \left[K_{s2} - P(H)\right]u'(H) - K_{s2}\varphi(H) = 0. \tag{24}$$

5 Generalized numerical solution

Consider functions $u(x)$, $\theta(x)$ and $\varphi(x)$ defined for x > 0. The Laplace transform of the displacements are expressed as the following integrals:

$$U(s) = L\left[u(x)\right] = \int_0^\infty u(x)e^{-sx}dx, \tag{25}$$

$$\Phi(s) = L\left[\theta(x)\right] = \int_0^\infty \theta(x)e^{-sx}dx, \tag{26}$$

$$\Psi(s) = L\left[\varphi(x)\right] = \int_0^\infty \varphi(x)e^{-sx}dx. \tag{27}$$

Applying the Laplace transforms to the system of equilibrium equations:

$$-(K_{s2} - P)s^2U(s) + K_{s2}s\Psi(s) = -(K_{s2} - P)su(0) - V(0), \tag{28}$$

$$\left(-K_{b1}s^2 + K_{s1}\right)\Phi(s) - K_{s1}\Psi(s) = -K_{b1}s\theta(0) - M_1(0), \tag{29}$$

$$\begin{aligned}&-K_{s2}sU(s) - K_{s1}\Phi(s) + \left[-K_{b2}s^2 + (K_{s1} + K_{s2})\right]\Psi(s)\\ &= -K_{s2}u(0) - K_{b2}s\varphi(0) - M_2(0).\end{aligned} \tag{30}$$

Solving the system of equations yields the Laplace transforms of the displacements in terms of the displacements and internal forces at the base of the generalized sandwich beam:

$$\begin{aligned}U(s) = &\left(\frac{1}{s}\right)u(0) - \frac{K_{s2}}{(K_{s2} - P)}\left[\frac{K_{s1}}{K_{b2}}\frac{1}{(s^2 - \xi)(s^2 + \beta)}\right]\theta(0) + \frac{K_{s2}}{(K_{s2} - P)}\left[\frac{s^2}{(s^2 - \xi)(s^2 + \beta)} - \frac{K_{s1}}{K_{b1}}\frac{1}{(s^2 - \xi)(s^2 + \beta)}\right]\varphi(0)\\ &- \frac{1}{K_{b1}}\frac{K_{s2}}{(K_{s2} - P)}\left[\frac{K_{s1}}{K_{b2}}\frac{1}{s(s^2 - \xi)(s^2 + \beta)}\right]M_1(0) + \frac{K_{s2}}{K_{b2}(K_{s2} - P)}\left[\frac{s}{(s^2 - \xi)(s^2 + \beta)} - \frac{K_{s1}}{K_{b1}}\frac{1}{s(s^2 - \xi)(s^2 + \beta)}\right]M_2(0)\\ &+ \frac{1}{(K_{s2} - P)}\left\{\frac{s^2}{(s^2 - \xi)(s^2 + \beta)} - \frac{K_{b1}(K_{s1} + K_{s2}) + K_{s1}K_{b2}}{K_{b1}K_{b2}}\frac{1}{(s^2 - \xi)(s^2 + \beta)} + \frac{K_{s1}K_{s2}}{K_{b1}K_{b2}}\frac{1}{s^2(s^2 - \xi)(s^2 + \beta)}\right\}V(0),\end{aligned} \tag{31}$$

$$\Phi(s)=\left[\frac{s^3}{\left(s^2-\xi\right)\left(s^2+\beta\right)}-\frac{K_{s1}K_{b2}-P\left(K_{s1}+K_{s2}\right)}{K_{b2}\left(K_{s2}-P\right)}\frac{s}{\left(s^2-\xi\right)\left(s^2+\beta\right)}\right]\theta(0)-\left[\frac{K_{s1}}{K_{b1}}\frac{s}{\left(s^2-\xi\right)\left(s^2+\beta\right)}\right]\varphi(0)$$
$$+\frac{1}{K_{b1}}\left[\frac{s^2}{\left(s^2-\xi\right)\left(s^2+\beta\right)}-\frac{K_{s1}K_{b2}-P\left(K_{s1}+K_{s2}\right)}{K_{b2}\left(K_{s2}-P\right)}\frac{1}{\left(s^2-\xi\right)\left(s^2+\beta\right)}\right]M_1(0) \tag{32}$$
$$-\frac{1}{K_{b2}}\left[\frac{K_{s1}}{K_{b1}}\frac{1}{\left(s^2-\xi\right)\left(s^2+\beta\right)}\right]M_2(0)+\frac{1}{\left(K_{s2}-P\right)}\left[\frac{K_{s1}K_{s2}}{K_{b1}K_{b2}}\frac{1}{s\left(s^2-\xi\right)\left(s^2+\beta\right)}\right]V(0),$$

$$\Psi(s)=-\left[\frac{K_{s1}}{K_{b2}}\frac{s}{\left(s^2-\xi\right)\left(s^2+\beta\right)}\right]\theta(0)+\left[\frac{s^3}{\left(s^2-\xi\right)\left(s^2+\beta\right)}-\frac{K_{s1}}{K_{b1}}\frac{s}{\left(s^2-\xi\right)\left(s^2+\beta\right)}\right]\varphi(0)$$
$$-\frac{1}{K_{b1}}\left[\frac{K_{s1}}{K_{b2}}\frac{1}{\left(s^2-\xi\right)\left(s^2+\beta\right)}\right]M_1(0)+\frac{1}{K_{b2}}\left[\frac{s^2}{\left(s^2-\xi\right)\left(s^2+\beta\right)}-\frac{K_{s1}}{K_{b1}}\frac{1}{\left(s^2-\xi\right)\left(s^2+\beta\right)}\right]M_2(0) \tag{33}$$
$$-\frac{1}{\left(K_{s2}-P\right)}\left[\frac{s}{\left(s^2-\xi\right)\left(s^2+\beta\right)}-\frac{K_{s1}K_{s2}}{K_{b1}K_{b2}}\frac{1}{s\left(s^2-\xi\right)\left(s^2+\beta\right)}\right]V(0),$$

where:

$$\xi=\frac{r_1+\sqrt{r_1^2+4r_2}}{2};\ \beta=\frac{-r_1+\sqrt{r_1^2+4r_2}}{2}, \tag{34}$$

$$r_1=\frac{K_{s1}K_{s2}\left(K_{b1}+K_{b2}\right)-P\left[K_{b1}\left(K_{s1}+K_{s2}\right)+K_{s1}K_{b2}\right]}{K_{b1}K_{b2}\left(K_{s2}-P\right)}, \tag{35}$$

$$r_2=\frac{PK_{s1}K_{s2}}{K_{b1}K_{b2}\left(K_{s2}-P\right)}. \tag{36}$$

The simplicity of the expressions in Eqs. (31)–(33) allows us to apply the inverse Laplace transform and directly obtain the expressions for the displacements $u(x)$, $\theta(x)$ and $\varphi(x)$. Expressing the displacements and internal forces in matrix form yields:

$$\begin{Bmatrix}u(x)\\ \theta(x)\\ \varphi(x)\\ M_1(x)\\ M_2(x)\\ V(x)\end{Bmatrix}=\begin{bmatrix}1 & t_{12}(x) & t_{13}(x) & t_{14}(x) & t_{15}(x) & t_{16}(x)\\ 0 & t_{22}(x) & t_{23}(x) & t_{24}(x) & t_{25}(x) & t_{26}(x)\\ 0 & t_{32}(x) & t_{33}(x) & t_{34}(x) & t_{35}(x) & t_{36}(x)\\ 0 & t_{42}(x) & t_{43}(x) & t_{44}(x) & t_{45}(x) & t_{46}(x)\\ 0 & t_{52}(x) & t_{53}(x) & t_{54}(x) & t_{55}(x) & t_{56}(x)\\ 0 & 0 & 0 & 0 & 0 & 1\end{bmatrix}\begin{Bmatrix}u(0)\\ \theta(0)\\ \varphi(0)\\ M_1(0)\\ M_2(0)\\ V(0)\end{Bmatrix}=\boldsymbol{T}(x)\begin{Bmatrix}u(0)\\ \theta(0)\\ \varphi(0)\\ M_1(0)\\ M_2(0)\\ V(0)\end{Bmatrix}, \tag{37}$$

where $\boldsymbol{T}(x)$ is the transfer matrix of the i-th element and the expressions of $t_{ij}(x)$ are shown in detail in Appendix A.

The relationship between forces and displacements of two consecutive elements can be expressed as:

$$\begin{Bmatrix}u\\ \theta\\ \varphi\\ M_1\\ M_2\\ V\end{Bmatrix}_i=\boldsymbol{T}_i\begin{Bmatrix}u\\ \theta\\ \varphi\\ M_1\\ M_2\\ V\end{Bmatrix}_{i-1}. \tag{38}$$

The following relationship is written as a result of successive operations between the base and the top of the building.

$$\begin{Bmatrix} u \\ \theta \\ \varphi \\ M_1 \\ M_2 \\ V \end{Bmatrix}_n = \prod_{k=n}^{1} \boldsymbol{T}_k \begin{Bmatrix} u(0) \\ \theta(0) \\ \varphi(0) \\ M_1(0) \\ M_2(0) \\ V(0) \end{Bmatrix}_1 = \boldsymbol{T} \begin{Bmatrix} u(0) \\ \theta(0) \\ \varphi(0) \\ M_1(0) \\ M_2(0) \\ V(0) \end{Bmatrix}_1, \tag{39}$$

where [19]:

$$\boldsymbol{T} = \prod_{k=n}^{1} \boldsymbol{T}_k. \tag{40}$$

By introducing the boundary conditions of the model (Eqs. (19)–(24)) into Eq. (39) and properly solving the determinant, a non-trivial solution is obtained by solving the eigenvalue problem of the following characteristic equation:

$$\left[t_{44}(x)t_{55}(x) - t_{45}(x)t_{54}(x)\right] + \frac{t_{42}(x)t_{55}(x) - t_{45}(x)t_{52}(x)}{K_R} = \mathbf{0}. \tag{41}$$

Evaluating Eq. (41) at $x = H$, solving the equation and performing algebraic operations, the global buckling critical load is obtained as:

$$q_{cr} = \left\{ \left\{ \left\{ \left[\frac{\pi^2 K_{b1}}{4H^2} \right]^{-1} + K_{s1}^{-1} \right\}^{-1} + \frac{\pi^2 K_{b2}}{4H^2} \right\}^{-1} + K_{s2}^{-1} \right\}^{-1}. \tag{42}$$

$$q_{cr} = \left\{ \left[\left(q_{cr,\text{global bending}}^{-1} + q_{cr,\text{global shear}}^{-1} \right)^{-1} + q_{cr,\text{local bending}} \right]^{-1} + q_{cr,\text{local shear}}^{-1} \right\}^{-1}, \tag{43}$$

where:

$$q_{cr,\text{global bending}} = \frac{\pi^2 K_{b1}}{4H^2}, \tag{44}$$

$$q_{cr,\text{global shear}} = K_{s1}, \tag{45}$$

$$q_{cr,\text{local bending}} = \frac{\pi^2 K_{b2}}{4H^2}, \tag{46}$$

$$q_{cr,\text{local shear}} = K_{s2}. \tag{47}$$

7 Procedure of computation

The computational procedure for conducting stability analyses of buildings featuring shear walls of considerable length is delineated as follows:

By solving and considering the lowest value, the vertical load P is obtained, and the global critical buckling load q_{cr} of the proposed continuous model is calculated by summing all the accumulated vertical loads across the stories of the structure.

6 Particular case

A commonly studied scenario in classical continuous models involves the application of a concentrated load at the top of the structure. In this particular case, an analytical closed-form solution is facilitated, since the resulting system of equilibrium equations has constant coefficients. In the instance of a building featuring a fixed base, the critical buckling load can be articulated in relation to its equivalent stiffnesses, elucidating their physical significance.

A detailed derivation of Eq. (42) is presented in Appendix B.

In other words:

- Determine the macroscopic properties of the building (K_{b1}, K_{s1}, K_{b2}, K_{s2}).
- Calculate the parameters r_1, r_2, ξ and β for each discretized element and in each iterative analysis.
- For the initial iteration, an approximation of the global buckling critical load is calculated using Föppl's theorem, with the vertical load P taken as the global buckling critical load obtained from Föppl's theorem divided by the number of stories in the structure.

$$q_{cr,\text{Föppl}} \approx \left(\frac{1}{q_{cr,1}} + \frac{1}{q_{cr,2}} + \frac{1}{q_{cr,3}} + \ldots + \frac{1}{q_{cr,n-1}} + \frac{1}{q_{cr,n}} \right)^{-1}. \tag{48}$$

- Calculate the modified transfer matrix for each story based on the characteristic stiffness and the parameters obtained in the previous steps.

- Obtain the transfer matrix for the entire building.
- Apply the boundary conditions.
- Obtain the non-trivial equation that solves the eigenvalue problem.

8 Numerical examples

To explore specific scenarios, this section is divided into five parts:

- Verification and Validation: Verify and validate the generalized sandwich beam and proposed solution method. Compare with the classic sandwich beam (established in the literature) and the finite element solution for accuracy.
- Buildings with Uniform Properties: Study 25 buildings with uniform properties along their height.
- Buildings with Variable Properties: Investigate 4 buildings with variable properties along their height.
- Parametric Analysis: Perform a parametric analysis to assess the range of application of the generalized sandwich beam.
- Effect of Soil Flexibility: Examine the impact of soil flexibility on the calculation of the global buckling critical load.

The outcomes derived from the generalized sandwich beam are juxtaposed with the numerical findings obtained through the finite element method. Notably, the finite element method, leverages the equivalent frame approach for the representation of shear walls and interconnecting beams. This comparison demonstrates a high degree of concordance between the results obtained from the generalized sandwich beam and those yielded by the finite element analysis.

8.1 Verification and validation

A detailed examination is conducted on a coupled shear wall configuration, specifically encompassing three bays (Fig. 4). The structural parameters include a story height h = 3 m, a wall thickness measuring t = 0.3 m, and variable cross-sections for the beams. In particular, the first and third bays exhibit cross-section dimensions of 0.3 m × 1.0 m, while the second bay features dimensions of 0.3 m × 0.5 m. The beams associated with these bays possess cross-sectional areas and second moments of area, with values for the first bay denoted as A_{b1} = 0.3 m^2 and I_{b1} = 0.025 m^4, and for the second bay as A_{b2} = 0.15 m^2 and I_{b2} = 0.003125 m^4. The material properties include a modulus of elasticity E = 30 GPa and a shear modulus G = 12.5 GPa [11].

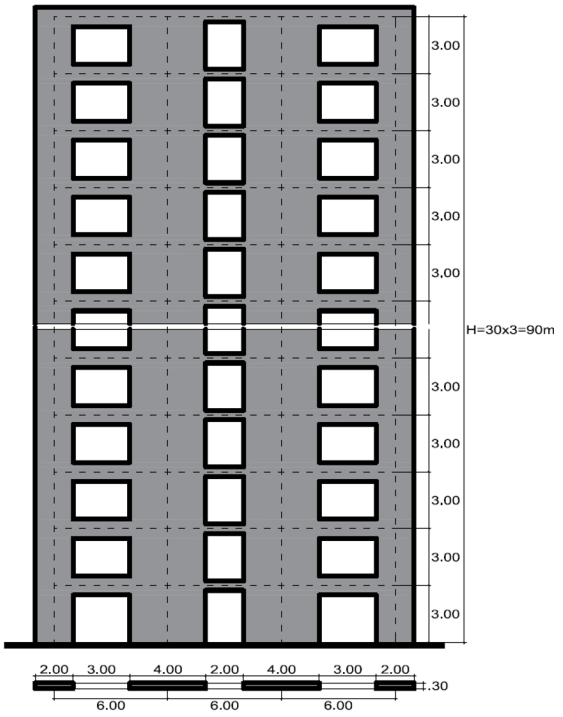

Fig. 4 Three-bay coupled shear wall [11]

The equivalent stiffnesses are calculated according to Eqs. (1)–(7): $K_{b1} = 3.564 \times 10^9$ kN × m^2, $K_{s1} = 7.194 \times 10^6$ kN, $K_{b2} = 1.014 \times 10^8$ kN × m^2, and $K_{s2} = 3.75 \times 10^7$ kN.

Fig. 5 shows the relative errors in the global critical buckling load obtained by comparing the results of the generalized sandwich beam (GSB beam), its variant with infinite local shear rigidity ($K_{s2} \to \infty$), and the classical sandwich beam (SWB beam), against the finite element method (FEM) solution. Clear differences are observed between the error profiles of the full GSB beam and the version without local shear deformation, demonstrating the significant contribution of the newly introduced shear mechanism in improving the accuracy. Specifically, the maximum error is reduced from +31.95% to +10.64% when local shear effects are included. Additionally, the approximate solution proposed in the literature [11] is compared with its exact counterpart derived from the GSB beam with $K_{s2} \to \infty$. Both approaches display similar behavior, with maximum errors of +37.59% (SWB beam) and +31.95% (GSB beam with $K_{s2} \to \infty$), respectively.

8.2 Building with uniform properties along the height

Within this segment, attention is directed towards the examination of 50 symmetrical theoretical structures braced vertically (Fig. 6). The vertical bracing system consists of seven interconnected shear walls, each with a thickness t = 0.4 m and a length L = 6 m. The modulus of

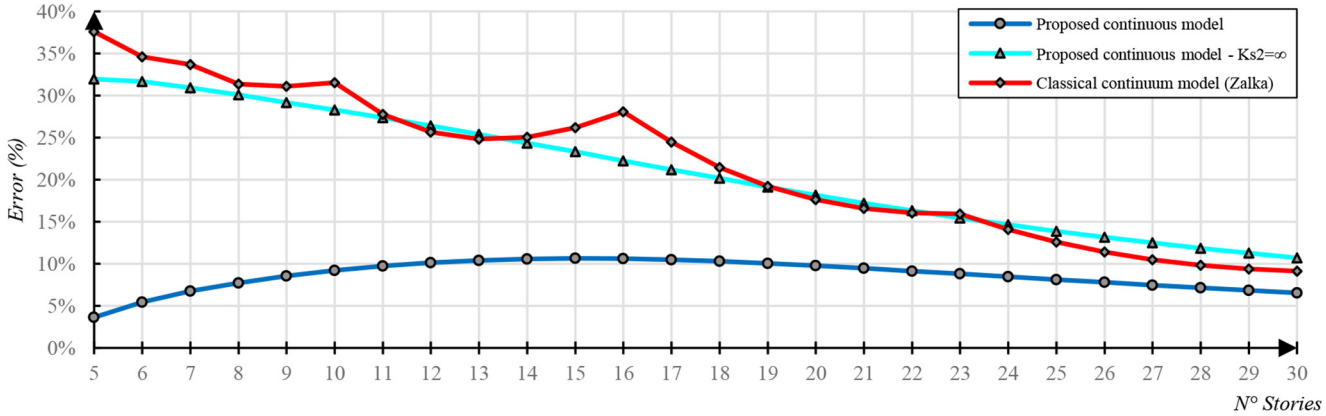

Fig. 5 Relative error in the global critical buckling load, obtained by comparing the results of the generalized sandwich beam (GSB beam), the GSB beam with infinite local shear rigidity ($K_{s2} \to \infty$), and the classical sandwich beam (SWB beam) [11], against the FEM reference solution

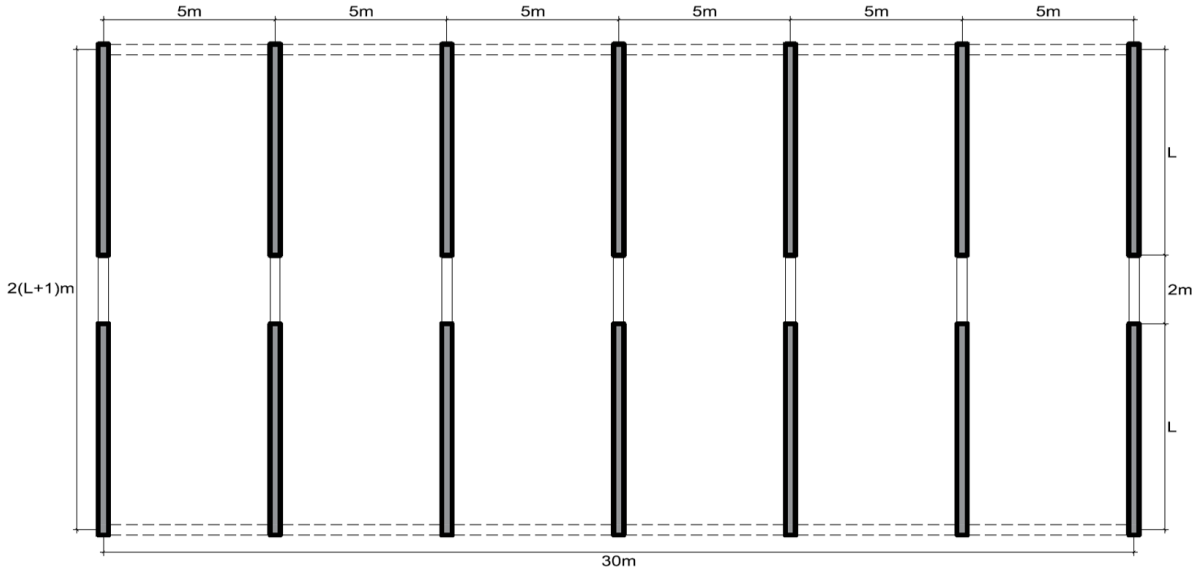

Fig. 6 Structural plan of the building analyzed

elasticity of the structure is denoted as E = 25 GPa, the shear modulus is G = 10.42 GPa, and the story height is kept constant at h = 3 m. Two distinct scenarios are analyzed, as described in Table 1, and their corresponding equivalent stiffnesses are presented in Table 2.

Figs. 7 (Case 1) and 8 (Case 2) illustrate the significant improvement in accuracy achieved using the generalized sandwich beam (GSB beam) compared to the classic sandwich beam (SWB beam). The SWB beam yielded errors of 27.12% and 37.48% for Cases 1 and 2, respectively, which decreased as the building height increased. In contrast, the errors obtained with the GSB beam are limited to a maximum of 4.38% and 3.81% for Cases 1 and 2, respectively, demonstrating a drastic reduction in error and an enhancement in structural safety.

Table 1 Section of the shear walls and the connecting beams for the two cases of analysis

Case	Shear wall section (m²)			Coupling beam section (m²)		
1	0.40	×	6.00	0.40	×	0.60
2	0.40	×	6.00	0.40	×	0.80

Table 2 Equivalent stiffness for cases 1 and 2

Case	K_{b1} (kN × m²)	K_{s1} (kN)	K_{b2} (kN × m²)	K_{s2} (kN)
1	13440000000	31653563	2491135412	291666667
2	13440000000	63912222	2461719042	291666667

8.3 Building with non-uniform properties along the height

To address the classic problem of buildings with variable properties throughout their height, this section verifies the application of the GSB beam. Specifically, a 30-story building from Section 8.2 is analyzed, divided into three equal sections with varying shear wall widths. The geometric

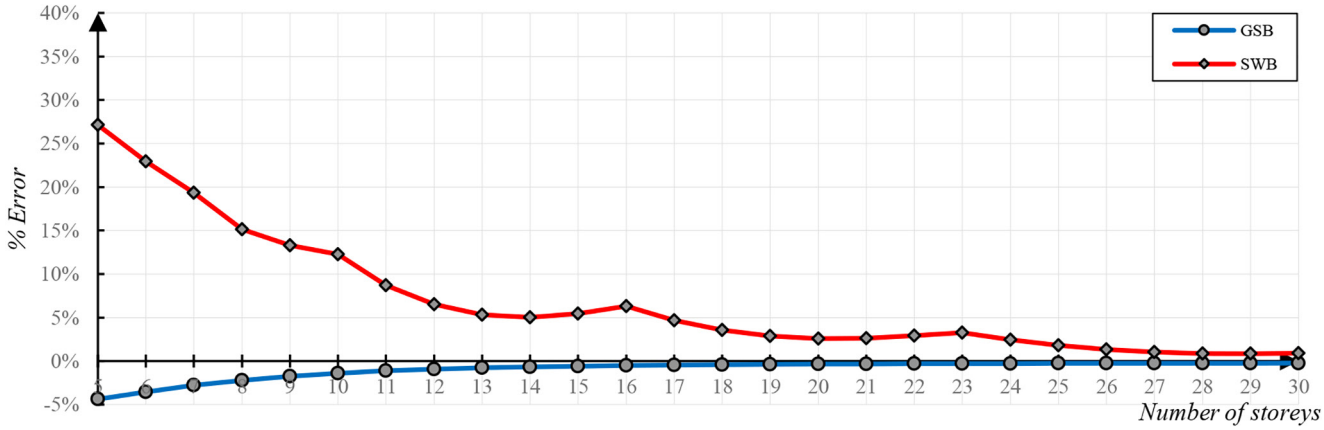

Fig. 7 Error profile obtained in the calculation of the critical load using the generalized sandwich beam (GSB beam) and the classical sandwich beam (SWB beam) [11] – Case 1

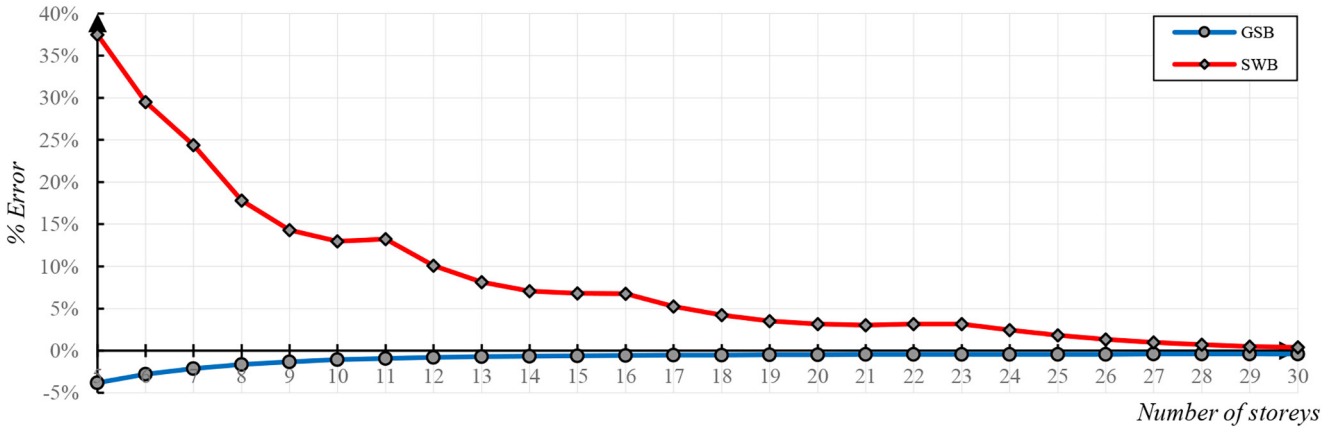

Fig. 8 Error profile obtained in the calculation of the critical load using the generalized sandwich beam (GSB beam) and the classical sandwich beam (SWB beam) [11] – Case 2

and material characteristics are detailed in Table 3 and the equivalent rigidities of the GSB beam in Table 4.

Table 5 summarizes the results of the critical load ratio calculation for the four types of buildings analyzed. The errors found are within a maximum of –4.23%,

Table 3 Summary of the four analysis cases for the 30-story building with variable properties

Case	Stories	Shear wall section (m^2)			Coupling beam section (m^2)		
	1–10	0.40	×	6.00	0.40	×	1.00
3	11–20	0.30	×	6.00	0.30	×	1.00
	21–30	0.20	×	6.00	0.20	×	1.00
	1–10	0.40	×	8.00	0.40	×	1.00
4	11–20	0.30	×	8.00	0.30	×	1.00
	21–30	0.20	×	8.00	0.20	×	1.00
	1–10	0.40	×	10.00	0.40	×	1.00
5	11–20	0.30	×	10.00	0.30	×	1.00
	21–30	0.20	×	10.00	0.20	×	1.00
	1–10	0.40	×	12.00	0.40	×	1.00
6	11–20	0.30	×	12.00	0.30	×	1.00
	21–30	0.20	×	12.00	0.20	×	1.00

which indicates that the application of the GSB beam provides a practical and accurate solution to the classic problem of buildings that have their properties varying along their height.

The results suggest that the GSB beam manages to adequately represent the complex global buckling behavior in buildings where their geometric properties vary in height. The errors are reasonable, which indicates the practicality and accuracy of the proposed approach.

8.4 Parametric analysis

A proposed method must be validated in order to be accepted as a reliable solution for structural engineers. To this end, a rigorous parametric analysis is conducted, involving 12 case studies with 26 variations each (Fig. 6). This approach enables the definition of the validity range of the GSB beam and its solution method. The height of the buildings varies between 15 and 90 m (from 5 to 30 stories), maintaining a consistent structural layout, as discussed in Section 8.1 (Fig. 6).

Table 6 summarizes the geometric characteristics for the parametric analyses. Twelve analysis cases are defined.

Table 4 Equivalent stiffness of the GSB beam for the four analysis cases

Case	Stories	K_{b1} (kN × m^2)	K_{s1} (kN)	K_{b2} (kN × m^2)	K_{s2} (kN)
	1–10	13440000000	104426132	2424774786	291666667
3	11–20	10080000000	103127150	1795959316	218750000
	21–30	6720000000	100623782	1168242113	145833333
	1–10	28000000000	165294635	5822602701	388888889
4	11–20	21000000000	163915888	4330526634	291666667
	21–30	14000000000	161226264	2839645943	194444444
	1–10	50400000000	239612777	11448166015	486111111
5	11–20	37800000000	238126185	8532854958	364583333
	21–30	25200000000	235207660	5618849666	243055556
	1–10	82320000000	327441672	19861409000	583333333
6	11–20	61740000000	325833028	14822875907	437500000
	21–30	41160000000	322662695	9785766904	291666667

Table 5 Ratio of critical loads calculated using the GSB beam – Cases 3–6

Case	FEM	GSB	Error
3	124.312	124.945	+0.51%
4	205.448	201.690	–1.83%
5	302.765	292.870	–3.27%
6	413.777	396.270	–4.23%

Table 6 Analysis cases and geometric characteristics of shear walls and connecting beams for parametric analysis

Case	Beam (m)		Shear wall (m)	
	Width (b)	Height (h)	Width (b)	Length (L)
CSW1	0.40	0.60	0.40	5.00
CSW2	0.40	0.80	0.40	5.00
CSW3	0.40	1.00	0.40	5.00
CSW4	0.40	0.60	0.40	7.50
CSW5	0.40	0.80	0.40	7.50
CSW6	0.40	1.00	0.40	7.50
CSW7	0.40	0.60	0.40	10.00
CSW8	0.40	0.80	0.40	10.00
CSW9	0.40	1.00	0.40	10.00
CSW10	0.40	0.60	0.40	12.50
CSW11	0.40	0.80	0.40	12.50
CSW12	0.40	1.00	0.40	12.50

All dimensions are the same except the length of the shear walls and the height of the connecting beams.

Tables 7, 8, and 9 provide a comprehensive overview of the results derived from the computation of the global critical buckling load for the building. The term "*Range of difference*" is employed to denote the span between the minimum and maximum error, "*Average absolute difference*" signifies the average of absolute errors, and "*Maximum difference*" articulates the highest error encountered in the parametric analysis.

Table 7 Summary of global buckling critical load accuracy analysis using the proposed continuum model

GSB beam	Range of difference [%]			Average absolute difference [%]	Maximum difference [%]
N° of stories ≥5	–4.40	-	–0.14	–0.76	–4.40

Table 8 Summary of the accuracy analysis of the critical global buckling load using the proposed continuum model adapted to the classical continuum model ($K_{s2} = \infty$)

GSB beam ($K_{s2} = \infty$)	Range of difference [%]			Average absolute difference [%]	Maximum difference [%]
N° of stories ≥5	+0.34	-	+128.81	+16.72	+128.81

Table 9 Summary of global buckling critical load accuracy analysis using classical continuum model [10]

SWB beam (Zalka [11])	Range of difference [%]			Average absolute difference [%]	Maximum difference [%]
N° of stories ≥5	+0.16	-	+144.71	+16.96	+144.71

To underline the superiority of the proposed continuous model, Table 7 shows the results obtained. To examine the errors arising from the omission of the local shear behavior, Table 8 shows the application of the GSB beam adapted to the SWB beam ($K_{s2} = \infty$). Furthermore, for validation purposes, the errors were calculated when using the SWB beam (Table 9) with the solution introduced by Zalka [11]. The findings underline that ignoring local shear stiffness in buildings with elongated shear walls significantly overestimates the results, leaning towards structural insecurity. The application of the GSB beam yields a maximum error of –4.40%, indicative of structural safety. In stark contrast, applying the SWB beam results in an alarming error of +144.71%.

Figs. 9, 10, and 11 illustrate the error trends identified during the computation of the global critical buckling load

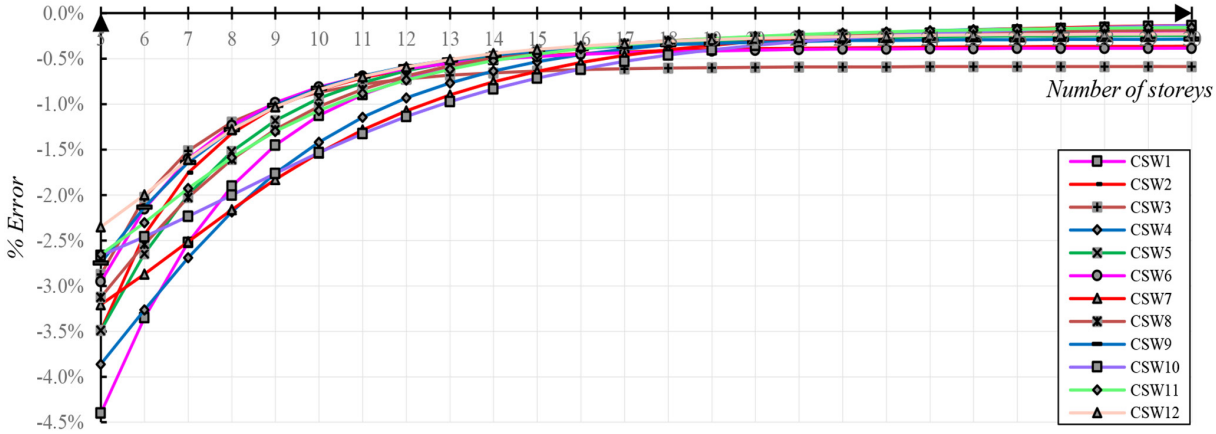

Fig. 9 Percentage error in the calculation of the critical load using the GSB beam

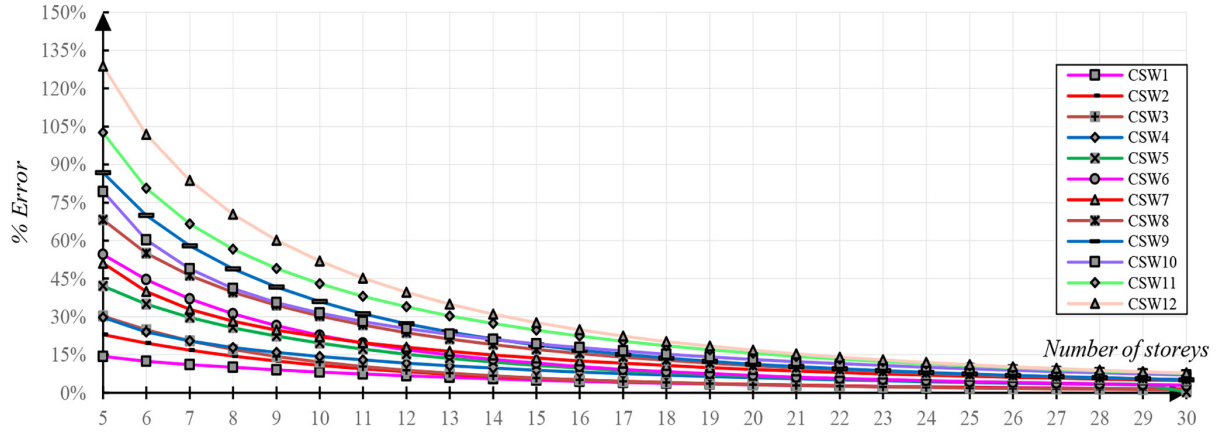

Fig. 10 Percentage error in the calculation of the critical load using the GSB beam adapted to the SWB beam ($K_{s2} = \infty$)

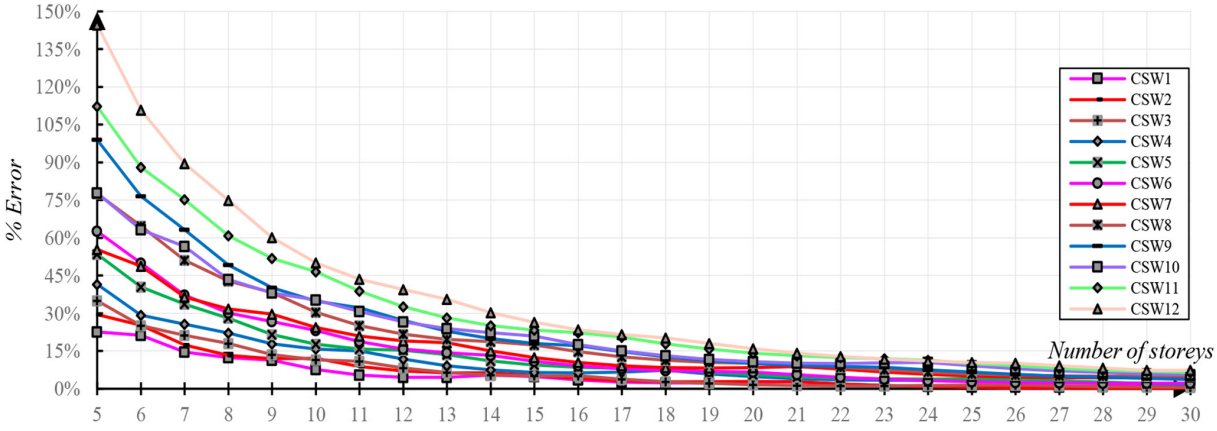

Fig. 11 Percentage error in the calculation of the critical load using the SWB beam [11]

of the building. It is noteworthy to observe that, in all instances, the error undergoes a substantial reduction as the height of the building increases.

To assess the trend of the proposed results in comparison with the finite element analysis, Figs. 12 (a)–(c) display the relationship between them. The closer the alignment of the data points to the 1:1 line, the higher the accuracy of the predictions. Notably, an outstanding correlation is observed for the GSB beam (Fig. 12 (a)), indicating remarkable agreement between the predicted and measured global critical buckling loads. Figs. 12 (b) and (c) show the global critical buckling loads predicted using the GSB beam adapted to the SWB beam ($K_{s2} = \infty$) and the SWB beam [11], respectively. In both analysis cases, the results reveal alarming errors that exceed acceptable thresholds within engineering criteria. The observed error trend reinforces the earlier statement

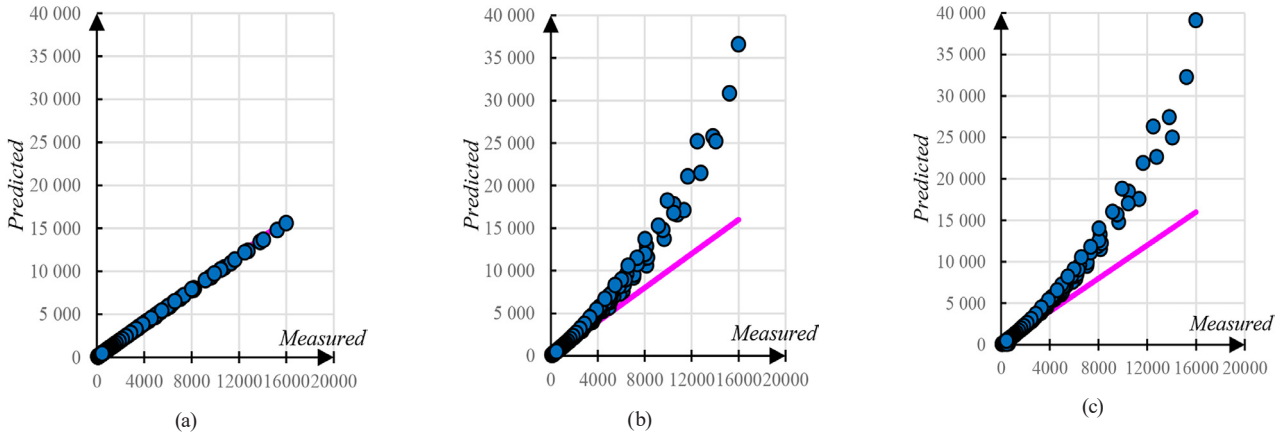

Fig. 12 Ratio of predicted global buckling critical load using the finite element model in SAP2000 versus: a) the GSB beam, b) the GSB beam adapted to the SWB beam ($K_{s2} = \infty$), and c) the SWB beam [11]

that, as global critical buckling loads increase (i.e., as building height decreases), the errors exhibit exponential growth.

8.5 Influence of soil flexibility in the calculation of the global buckling critical load

The mathematical formulation introduced in this study demonstrated that the critical global buckling load is influenced solely by the rotational stiffness of the soil. To assess soil flexibility, four distinct types of soil are considered, following the classifications proposed by Huergo and Hernández [33]. Table 10 presents a summary of soil parameters and foundation characteristics.

The soil's flexibility is characterized by incorporating four soil types based on the classification by Huergo and Hernández [33], as outlined in Table 10: "Hard rock", "Dense soil", "Stiff soil" and "Soft soil". Specifically, "Hard rock" signifies soil with a fixed base behavior, serving as a reference for comparing and analyzing eigenvalues using the modified transfer matrix method proposed in this study.

The analyzed building corresponds to cases 1 and 2 in Section 8.2. To assess how soil flexibility impacts the potential behaviors of the building, variations in building height were considered, ranging from 5 m to 90 m. The building's characteristic rigidities and geometric properties are provided in detail in Table 2.

Figs. 13 and 14 illustrate the impact of soil flexibility on the calculation of global critical buckling loads

Table 10 Parameters of the soils to evaluate their influence on the critical load due to global buckling

Soil type	vs	ρ_s (kg/m^3)	V_s (m/s)	G_s (GPa)	k_t (GN/m)	k_θ (TN-m)
Hard rock	0.25	2700	2722	20	1140	139
Dense	0.33	2400	500	0.6	35.9	4.66
Stiff	0.48	1900	300	0.171	11.3	1.71
Soft	0.49	1800	100	0.018	1.19	0.184

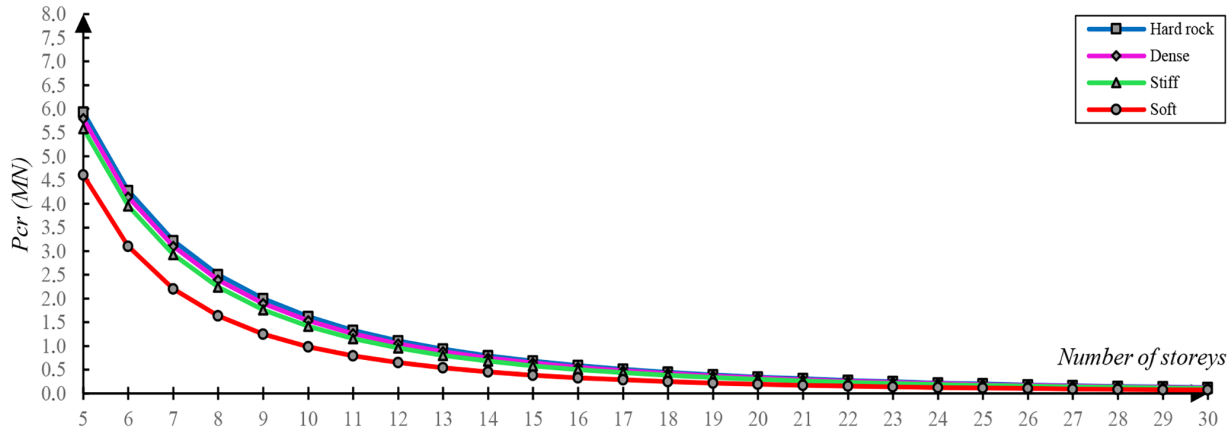

Fig. 13 Global buckling critical loads considering the rotational flexibility of the soil – Case 1

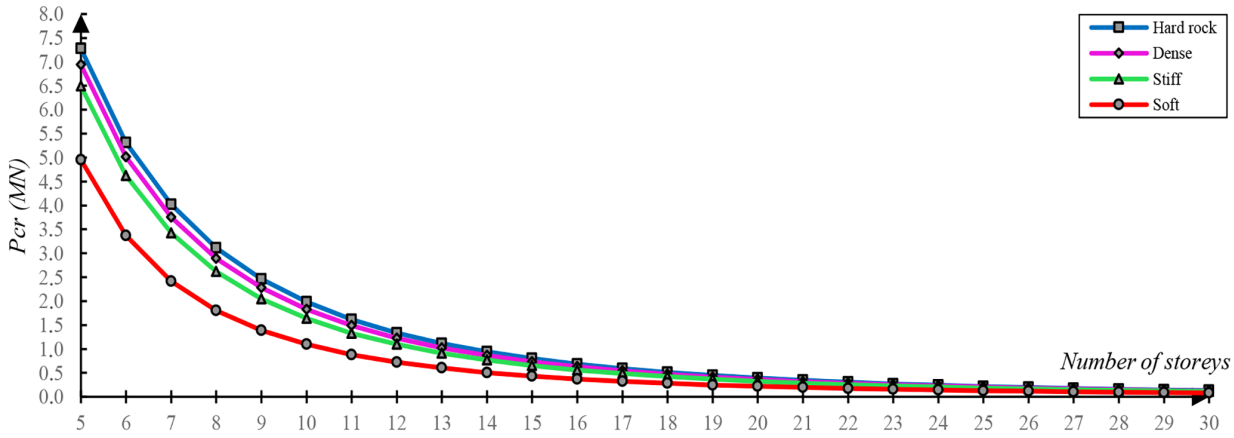

Fig. 14 Global buckling critical loads considering the rotational flexibility of the soil – Case 2

for Cases 1 and 2, respectively. For both cases, the trend exhibits an exponential pattern that decreases as the building height increases.

Figs. 15 and 16 show the change in the ratio P_{cr} / $P_{cr,\text{Hard rock}}$ as the building height increases. In both cases, the more flexible soil exhibits a greater ratio. Specifically, a maximum ratio of –43.89% and –46.09% was identified for Cases 1 and 2, respectively.

9 Conclusions and future work

This paper presents a novel generalized sandwich-type continuous beam and its solution methods for determining the global buckling critical load in both uniform and non-uniform buildings subjected to vertical loads – either concentrated or distributed along the height of the structure. Furthermore, the supporting soil flexibility is considered to allow for a simplified representation of the soil

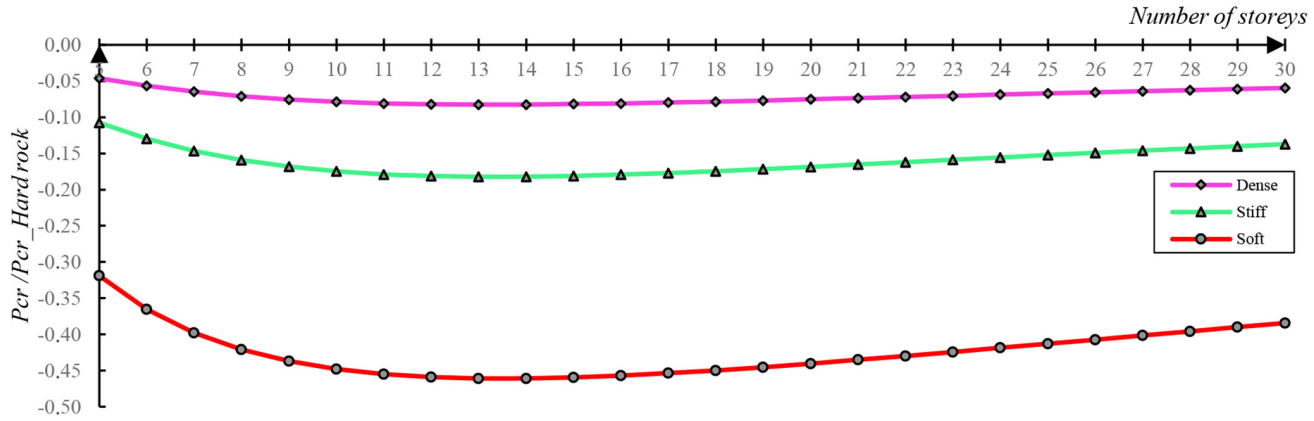

Fig. 15 Percentage change in global buckling critical load for rotational flexibility compared to hard rock type soil that is considered fixed – Case 1

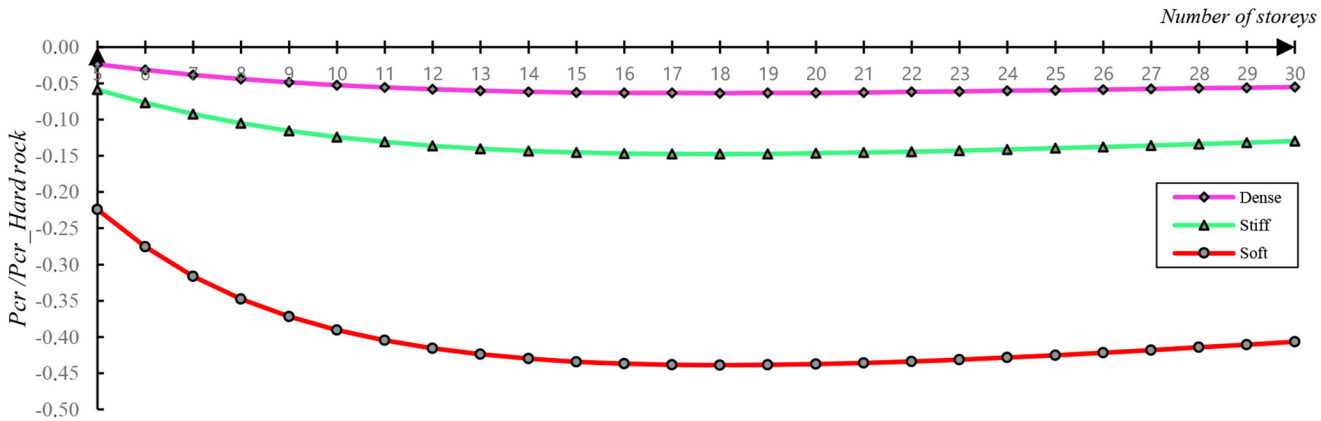

Fig. 16 Percentage change in global buckling critical load for rotational flexibility compared to hard rock type soil that is considered fixed – Case 2

– structure interaction effect. The main findings and contributions to the existing literature are outlined below:

- The generalized sandwich-type continuous beam (GSB beam) is derived from the extension of the classical sandwich beam (SWB beam) by coupling it in series with a shear beam, introducing a new kinematic rotation field and a deformation mechanism associated with the local shear of the walls – an effect often neglected in the classical formulation. This enhancement enables an accurate representation of the four deformation mechanisms involved in the global buckling analysis of buildings.
- A numerical solution method has been proposed that modifies the classical transfer matrix approach. This modification allows for the analytical calculation of the transfer matrix coefficients, significantly reducing computational cost as the matrix size and the number of discretizations increase. The proposed numerical method is capable of generalizing the calculation of the global critical buckling load for buildings with uniform and variable geometric and material properties under arbitrary vertical loads.
- It has been demonstrated, for the continuous beam with fixed and flexible base, that the translational stiffness does not influence the calculations of global critical buckling loads.
- The GSB beam and solution method have been validated through a rigorous parametric analysis, revealing a maximum error of –4.40% compared to the SWB beam error of +144.71% [11], which is unacceptable under engineering criteria, non-conservative, and unsafe for practical application. Conversely, the excellent accuracy achieved with the GSB beam ensures its safe application in engineering practice, providing results that are acceptable, precise, and on the conservative side of structural safety.
- The impact of soil flexibility on critical load calculations has been studied, revealing a negative influence that reduces the values up to –46.09% in the cases analyzed.

This paper enables the accurate calculation of the ratio between the global critical buckling load and the total building weight to assess the necessity of including second-order effects. However, it is necessary to propose analytical and numerical expressions to evaluate P-Delta second-order effects according to design codes, using dimensionless parameters such as α y γ_z [34]. Furthermore, the next step will focus on extending the model to nonlinear buckling analysis under seismic excitation and incorporating the behavior of viscoelastic soil.

Credit authorship contribution statement

Mao Cristian Pinto-Cruz: Responsible for everything (single author paper).

Declaration of Competing Interest

The author declares that he has no known competing financial interests or personal relationships that could have appeared to influence the work reported in this paper.

Acknowledgment

This research was made possible by the support of Jesus Christ during the key moments of my life. I dedicate this work to my beloved daughter, Zoé Juliette Pinto Pereira, whose presence strengthens me every day of my life. *We do not pray to have all the answers; we pray to see the world as God sees it – to truly see it. In the Lord's Prayer, the prayer Jesus taught us, there are no requests for knowledge, but rather for God's will to be done on earth. Rivers of ink have been spilled about Jesus' prayer – how we should pray, how to pray effectively, and so on. But the point is that we can be in direct connection and communication with the all-knowing God. Not so that He tells us everything, but so that we may know Him and understand what He desires.* Jesus is the question. – Alex Sampedro

"*And going a little farther he fell on his face and prayed, saying, 'My Father, if it be possible, let this cup pass from me; nevertheless, not as I will, but as you will.*'" (Matthew 26:39)

"*Beloved, do not be surprised at the fiery trial when it comes upon you to test you, as though something strange were happening to you. But rejoice insofar as you share Christ's sufferings, that you may also rejoice and be glad when his glory is revealed.*" (1 Peter 4:12–13)

References

[1] Hamed, M. A., Abo-bakr, R. M., Mohamed, S. A., Eltaher, M. A. "Influence of axial load function and optimization on static stability of sandwich functionally graded beams with porous core", Engineering with Computers, 36, pp. 1929–1946, 2020. https://doi.org/10.1007/s00366-020-01023-w

[2] Chitty, L. "On the cantilever composed of a number of parallel beams interconnected by cross bars", The London, Edinburgh, and Dublin Philosophical Magazine and Journal of Science, 38(285), pp. 685–699, 1947. https://doi.org/10.1080/14786444708521646

[3] Chitty, L., Wan, W. Y. "Tall building structures under wind load", presented at Proceedings of the 7th International Congress for Applied Mechanics, London, UK, Jan, 22, 1948.

[4] Potzta, G., Kollár, L. P. "Analysis of building structures by replacement sandwich beams", International Journal of Solids and Structures, 40(3), pp. 535–553, 2003. https://doi.org/10.1016/S0020-7683(02)00622-4

[5] Aksogan, O., Arslan, H. M., Choo, B. S. "Forced vibration analysis of stiffened coupled shear walls using continuous connection method", Engineering Structures, 25(4), pp. 499–506, 2003. https://doi.org/10.1016/S0141-0296(02)00192-X

[6] Aksogan, O., Turkozer, C. D., Emsen, E., Resatoglu, R. "Dynamic analysis of non-planar coupled shear walls with stiffening beams using continuous connection method", Thin-Walled Structures, 82, pp. 95–104, 2014. https://doi.org/10.1016/j.tws.2014.03.018

[7] Emsen, E., Aksogan, O. "Static analysis of non-planar coupled shear walls with stepwise changes in geometrical properties using continuous connection method", Thin-Walled Structures, 56, pp. 21–32, 2012. https://doi.org/10.1016/j.tws.2012.03.006

[8] Resatoglu, R., Aksogan, O., Emsen, E. "Static analysis of laterally arbitrarily loaded non-planar non-symmetrical coupled shear walls", Thin-Walled Structures, 48(9), pp. 696–708, 2010. https://doi.org/10.1016/j.tws.2010.04.009

[9] Zalka, K. A. "A simple method for the deflection analysis of tall wall-frame building structures under horizontal load", The Structural Design of Tall and Special Buildings, 18(3), pp. 291–311, 2007. https://doi.org/10.1002/tal.410

[10] Zalka, K. A. "Maximum deflection of symmetric wall-frame buildings", Periodica Polytechnica Civil Engineering, 57(2), pp. 173–184, 2013. https://doi.org/10.3311/PPci.7172

[11] Zalka, K. "Structural analysis of multi-storey buildings", CRC Press, Taylor & Francis Group, 2020. ISBN 978-0367350253

[12] Xu, G., Li, A. "Research on the response of concrete cavity shear wall under lateral load", The Structural Design of Tall and Special Buildings, 28(3), e1577, 2019. https://doi.org/10.1002/tal.1577

[13] Hu, H.-S., Wang, R.-T., Guo, Z.-X., Shahrooz, B. M. "A generalized method for estimating drifts and drift components of tall buildings under lateral loading", The Structural Design of Tall and Special Buildings, 29(2), e1688, 2020. https://doi.org/10.1002/tal.1688

[14] Tong, G., Lin, C. "Relations between buckling and vibrational characteristics of coupled shear walls", Structures, 31, pp. 1173–1184, 2021. https://doi.org/10.1016/j.istruc.2021.01.084

[15] Wang, R.-T., Hu, H.-S., Guo, Z.-X. "Analytical study of stiffened multibay planar coupled shear walls", Engineering Structures, 244, 112770, 2021. https://doi.org/10.1016/j.engstruct.2021.112770

[16] Zhang, L., Liu, T., Chen, Y. "Calculations of additional axial force and coupling ratio for coupled shear walls", Structures, 47, pp. 1531–1547, 2023. https://doi.org/10.1016/j.istruc.2022.11.126

[17] Chesnais, C. "Dynamics of unbraced reticular media: application to buildings", Level (PhD), Central School of Lyon, 2010.

[18] Chesnais, C., Boutin, C., Hans, S. "Structural dynamics and generalized continua", Springer Berlin Heidelberg, 7, pp. 57–76, 2011. https://doi.org/10.1007/978-3-642-19219-7_3

[19] Bozdogan, K. B., Ozturk, D. "A method for static and dynamic analyses of stiffened multi-bay coupled shear walls", Structural Engineering and Mechanics, 28(4), pp. 479–489, 2008. https://doi.org/10.12989/sem.2008.28.4.479

[20] Bozdogan, K. B., Ozturk, D., Nuhoglu, A. "An approximate method for static and dynamic analyses of multi-bay coupled shear walls", The Structural Design of Tall and Special Buildings, 18(1), pp. 1–12, 2009. https://doi.org/10.1002/tal.390

[21] Bozdogan, K. B. "An approximate method for static and dynamic analyses of symmetric wall-frame buildings", The Structural Design of Tall and Special Buildings, 18(3), pp. 279–290, 2009. https://doi.org/10.1002/tal.409

[22] Bozdogan, K. B., Ozturk, D. "An approximate method for lateral stability analysis of wall-frame buildings including shear deformations of walls", Sadhana, 35(3), pp. 241–253, 2010. https://doi.org/10.1007/s12046-010-0008-y

[23] Bozdogan, K. B., Ozturk, D. "Vibration analysis of asymmetric shear wall-frame structures using the transfer matrix method", Iranian Journal of Science and Technology-Transactions of Civil Engineering, 36(1), pp. 1–12, 2012.

[24] Bozdogan, K. B. Ozturk, D. "A method for dynamic analysis of frame-hinged shear wall structures", Earthquakes and Structures, 11(1), pp. 45–61, 2016. https://doi.org/10.12989/eas.2016.11.1.045

[25] Kara, D., Bozdogan, K. B., Keskin, E. "A simplified method for free vibration analysis of wall-frames considering soil structure interaction", Structural Engineering and Mechanics, 77(1), pp. 37–46, 2021. https://doi.org/10.12989/sem.2021.77.1.037

[26] Xia, G., Shu, W., Stanciulescu, I. "Efficient analysis of shear wall-frame structural systems", Engineering Computations, 36(6), pp. 2084–2110, 2019. https://doi.org/10.1108/EC-12-2018-0568

[27] Pinto Cruz, M. C. "A novel generalized sandwich-type replacement beam for static analysis of tall buildings: Inclusion of local shear deformation of walls", Thin-Walled Structures, 190, 110967, 2023. https://doi.org/10.1016/j.tws.2023.110967

[28] Pinto-Cruz, M. C. "A novel correction factor for local shear deformation mechanisms in static analysis of coupled shear walls", Journal of the Brazilian Society of Mechanical Sciences and Engineering, 47, 161, 2025. https://doi.org/10.1007/s40430-025-05396-1

[29] Pinto-Cruz, M. C. "Dynamic analysis of uniform and variable buildings with flexible base: Inclusion of local shear deformation of walls", Engineering Structures, 327, 119588, 2025. https://doi.org/10.1016/j.engstruct.2024.119588

[30] Pinto-Cruz, M. C. "Analytical solutions for global buckling analysis of regular buildings: Inclusion of local shear deformation of walls", Structures, 69, 107370, 2024. https://doi.org/10.1016/j.istruc.2024.107370

[31] Pinto-Cruz, M. C. "Analytical and numerical solution of generalized static analysis of tall buildings: double-beam systems Timoshenko", Journal of the Brazilian Society of Mechanical Sciences and Engineering, 46, 368, 2024.
https://doi.org/10.1007/s40430-024-04809-x

[32] Yoo, C. H., Lee, S. C. "Stability of structures: principles and applications", Butterworth-Heinemann, 2011. ISBN 978-0-12-385122-2
https://doi.org/10.1016/C2010-0-66075-5

[33] Huergo, I. F., Hernández, H. "Coupled-two-beam discrete model for dynamic analysis of tall buildings with tuned mass dampers including soil–structure interaction", The Structural Design of Tall and Special Buildings, 29(1), e1683, 2020.
https://doi.org/10.1002/tal.1683

[34] ABNT (Associação Brasileira de Normas Técnicas) "NBR 6118: Projeto de estruturas de concreto", (English title), ABNT, 2023. ISBN 978-85-07-09632-0 (in Portuguese)

Appendix A Transfer matrix coefficients

The expressions of $t_{ij}(x)$ for $i, j = 1, 2, 3, 4, 5, 6$ are shown below:

$$t_{12}(x) = -\frac{K_{s1}K_{s2}}{K_{b2}(K_{s2}-P)(\xi+\beta)}\left[\frac{\sinh\left(\sqrt{\xi}x\right)}{\sqrt{\xi}} - \frac{\sin\left(\sqrt{\beta}x\right)}{\sqrt{\beta}}\right], \tag{A1}$$

$$t_{13}(x) = \frac{K_{s2}}{(K_{s2}-P)(\xi+\beta)}\left[\left(\sqrt{\xi} - \frac{K_{s1}}{K_{b1}}\frac{1}{\sqrt{\xi}}\right)\sinh\left(\sqrt{\xi}x\right) + \left(\sqrt{\beta} + \frac{K_{s1}}{K_{b1}}\frac{1}{\sqrt{\beta}}\right)\sin\left(\sqrt{\beta}x\right)\right], \tag{A2}$$

$$t_{14}(x) = -\frac{K_{s1}K_{s2}}{K_{b1}K_{b2}(K_{s2}-P)}\left\{-\frac{1}{\xi\beta} + \frac{1}{(\xi+\beta)}\left[\frac{\cosh\left(\sqrt{\xi}x\right)}{\xi} + \frac{\cos\left(\sqrt{\beta}x\right)}{\beta}\right]\right\}, \tag{A3}$$

$$t_{15}(x) = \frac{1}{K_{b2}(K_{s2}-P)}\left\{\frac{K_{s1}K_{s2}}{K_{b1}}\frac{1}{\xi\beta} + \frac{K_{s2}}{(\xi+\beta)}\left[\left(1-\frac{K_{s1}}{K_{b1}}\frac{1}{\xi}\right)\cosh\left(\sqrt{\xi}x\right) - \left(1+\frac{K_{s1}}{K_{b1}}\frac{1}{\beta}\right)\cos\left(\sqrt{\beta}x\right)\right]\right\}, \tag{A4}$$

$$t_{16}(x) = \frac{1}{(K_{s2}-P)}\left\{\begin{aligned}&-\frac{K_{s1}K_{s2}}{K_{b1}K_{b2}}\frac{1}{\xi\beta}x + \frac{1}{(\xi+\beta)}\left[\sqrt{\xi} - \frac{K_{b1}(K_{s1}+K_{s2})+K_{s1}K_{b2}}{K_{b1}K_{b2}}\frac{1}{\sqrt{\xi}} + \frac{K_{s1}K_{s2}}{K_{b1}K_{b2}}\frac{1}{\xi\sqrt{\xi}}\right]\sinh\left(\sqrt{\xi}x\right)\\ &+\frac{1}{(\xi+\beta)}\left[\sqrt{\beta} + \frac{K_{b1}(K_{s1}+K_{s2})+K_{s1}K_{b2}}{K_{b1}K_{b2}}\frac{1}{\sqrt{\beta}} + \frac{K_{s1}K_{s2}}{K_{b1}K_{b2}}\frac{1}{\beta\sqrt{\beta}}\right]\sin\left(\sqrt{\beta}x\right)\end{aligned}\right\}, \tag{A5}$$

$$t_{22}(x) = \frac{1}{(\xi+\beta)}\left\{\left[\xi - \frac{K_{s1}K_{s2}-P(K_{s1}+K_{s2})}{K_{b2}(K_{s2}-P)}\right]\cosh\left(\sqrt{\xi}x\right) + \left[\beta + \frac{K_{s1}K_{s2}-P(K_{s1}+K_{s2})}{K_{b2}(K_{s2}-P)}\right]\cos\left(\sqrt{\beta}x\right)\right\}, \tag{A6}$$

$$t_{23}(x) = -\frac{K_{s1}}{K_{b1}}\frac{1}{(\xi+\beta)}\left[\cosh\left(\sqrt{\xi}x\right) - \cos\left(\sqrt{\beta}x\right)\right], \tag{A7}$$

$$t_{24}(x) = \frac{1}{K_{b1}(\xi+\beta)}\left\{\left[\sqrt{\xi} - \frac{K_{s1}K_{s2}-P(K_{s1}+K_{s2})}{K_{b2}(K_{s2}-P)\sqrt{\xi}}\right]\sinh\left(\sqrt{\xi}x\right) + \left[\sqrt{\beta} + \frac{K_{s1}K_{s2}-P(K_{s1}+K_{s2})}{K_{b2}(K_{s2}-P)\sqrt{\beta}}\right]\sin\left(\sqrt{\beta}x\right)\right\}, \tag{A8}$$

$$t_{25}(x) = -\frac{K_{s1}}{K_{b1}K_{b2}(\xi+\beta)}\left[\frac{\sinh\left(\sqrt{\xi}x\right)}{\sqrt{\xi}} - \frac{\sin\left(\sqrt{\beta}x\right)}{\sqrt{\beta}}\right], \tag{A9}$$

$$t_{26}(x)=\frac{K_{s1}K_{s2}}{K_{b1}K_{b2}(K_{s2}-P)}\left\{-\frac{1}{\xi\beta}+\frac{1}{(\xi+\beta)}\left[\frac{\cosh\left(\sqrt{\xi}x\right)}{\xi}+\frac{\cos\left(\sqrt{\beta}x\right)}{\beta}\right]\right\}, \tag{A10}$$

$$t_{32}(x)=-\frac{K_{s1}}{K_{b2}(\xi+\beta)}\left[\cosh\left(\sqrt{\xi}x\right)-\cos\left(\sqrt{\beta}x\right)\right], \tag{A11}$$

$$t_{33}(x)=\frac{1}{(\xi+\beta)}\left[\left(\xi-\frac{K_{s1}}{K_{b1}}\right)\cosh\left(\sqrt{\xi}x\right)+\left(\beta+\frac{K_{s1}}{K_{b1}}\right)\cos\left(\sqrt{\beta}x\right)\right], \tag{A12}$$

$$t_{34}(x)=-\frac{K_{s1}}{K_{b1}K_{b2}(\xi+\beta)}\left[\frac{\sinh\left(\sqrt{\xi}x\right)}{\sqrt{\xi}}-\frac{\sin\left(\sqrt{\beta}x\right)}{\sqrt{\beta}}\right], \tag{A13}$$

$$t_{35}(x)=\frac{1}{K_{b2}(\xi+\beta)}\left[\left(\sqrt{\xi}-\frac{K_{s1}}{K_{b1}}\frac{1}{\sqrt{\xi}}\right)\sinh\left(\sqrt{\xi}x\right)+\left(\sqrt{\beta}+\frac{K_{s1}}{K_{b1}}\frac{1}{\sqrt{\beta}}\right)\sin\sqrt{\beta}x\right], \tag{A14}$$

$$t_{36}(x)=\frac{1}{(K_{s2}-P)}\left[-\frac{K_{s1}K_{s2}}{K_{b1}K_{b2}}\frac{1}{\xi\beta}-\frac{K_{s2}}{K_{b2}}\frac{1}{(\xi+\beta)}\left(1-\frac{K_{s1}}{K_{b1}}\frac{1}{\xi}\right)\cosh\left(\sqrt{\xi}x\right)+\frac{K_{s2}}{K_{b2}}\frac{1}{(\xi+\beta)}\left(1+\frac{K_{s1}}{K_{b1}}\frac{1}{\beta}\right)\cos\left(\sqrt{\beta}x\right)\right], \tag{A15}$$

$$t_{42}(x)=\frac{K_{b1}}{(\xi+\beta)}\left\{\sqrt{\xi}\left[\xi-\frac{K_{s1}K_{s2}-P(K_{s1}+K_{s2})}{K_{b2}(K_{s2}-P)}\right]\sinh\left(\sqrt{\xi}x\right)-\sqrt{\beta}\left[\beta+\frac{K_{s1}K_{s2}-P(K_{s1}+K_{s2})}{K_{b2}(K_{s2}-P)}\right]\sin\left(\sqrt{\beta}x\right)\right\}, \tag{A16}$$

$$t_{43}(x)=-\frac{K_{s1}}{(\xi+\beta)}\left[\sqrt{\xi}\sinh\left(\sqrt{\xi}x\right)+\sqrt{\beta}\sin\left(\sqrt{\beta}x\right)\right], \tag{A17}$$

$$t_{44}(x)=\frac{1}{(\xi+\beta)}\left\{\sqrt{\xi}\left[\sqrt{\xi}-\frac{K_{s1}K_{s2}-P(K_{s1}+K_{s2})}{K_{b2}(K_{s2}-P)\sqrt{\xi}}\right]\cosh\left(\sqrt{\xi}x\right)+\sqrt{\beta}\left[\sqrt{\beta}+\frac{K_{s1}K_{s2}-P(K_{s1}+K_{s2})}{K_{b2}(K_{s2}-P)\sqrt{\beta}}\right]\cos\left(\sqrt{\beta}x\right)\right\}, \tag{A18}$$

$$t_{45}(x)=-\frac{K_{s1}}{K_{b2}(\xi+\beta)}\left[\cosh\left(\sqrt{\xi}x\right)-\cos\left(\sqrt{\beta}x\right)\right], \tag{A19}$$

$$t_{46}(x)=\frac{K_{s1}K_{s2}}{K_{b2}(\xi+\beta)(K_{s2}-P)}\left[\frac{\sinh\left(\sqrt{\xi}x\right)}{\sqrt{\xi}}-\frac{\sin\left(\sqrt{\beta}x\right)}{\sqrt{\beta}}\right], \tag{A20}$$

$$t_{52}(x)=-\frac{K_{s1}}{(\xi+\beta)}\left[\sqrt{\xi}\sinh\left(\sqrt{\xi}x\right)+\sqrt{\beta}\sin\left(\sqrt{\beta}x\right)\right], \tag{A21}$$

$$t_{53}(x)=\frac{K_{b2}}{(\xi+\beta)}\left[\sqrt{\xi}\left(\xi-\frac{K_{s1}}{K_{b1}}\right)\sinh\left(\sqrt{\xi}x\right)-\sqrt{\beta}\left(\beta+\frac{K_{s1}}{K_{b1}}\right)\sin\left(\sqrt{\beta}x\right)\right], \tag{A22}$$

$$t_{54}(x)=-\frac{K_{s1}}{K_{b1}(\xi+\beta)}\left[\cosh\left(\sqrt{\xi}x\right)-\cos\left(\sqrt{\beta}x\right)\right], \tag{A23}$$

$$t_{55}(x)=\frac{1}{(\xi+\beta)}\left[\sqrt{\xi}\left(\sqrt{\xi}-\frac{K_{s1}}{K_{b1}}\frac{1}{\sqrt{\xi}}\right)\cosh\left(\sqrt{\xi}x\right)+\sqrt{\beta}\left(\sqrt{\beta}+\frac{K_{s1}}{K_{b1}}\frac{1}{\sqrt{\beta}}\right)\cos\left(\sqrt{\beta}x\right)\right], \tag{A24}$$

$$t_{56}(x)=-\frac{K_{s2}}{(\xi+\beta)(K_{s2}-P)}\left[\sqrt{\xi}\left(1-\frac{K_{s1}}{K_{b1}}\frac{1}{\xi}\right)\sinh\left(\sqrt{\xi}x\right)+\sqrt{\beta}\left(1+\frac{K_{s1}}{K_{b1}}\frac{1}{\beta}\right)\sin\left(\sqrt{\beta}x\right)\right]. \tag{A25}$$

Appendix B Detailed Derivation of Eq. (42)

The characteristic Eq. (41) can be rewritten using Eqs. (A18), (A24), (A19), and (A23) as follows:

$$t_{44}(x)t_{55}(x)-t_{45}(x)t_{54}(x)=$$
$$\frac{1}{(\xi+\beta)^2}\left\{\begin{array}{l}\left[\left(\xi-m\right)\left(\xi-\frac{K_{s1}}{K_{b1}}\right)-\left(\frac{K_{s1}}{K_{b2}}\right)^2\right]\cosh^2\left(\sqrt{\xi}H\right)+\left[\left(\beta+m\right)\left(\beta+\frac{K_{s1}}{K_{b1}}\right)-\left(\frac{K_{s1}}{K_{b2}}\right)^2\right]\cos^2\left(\sqrt{\beta}H\right)\\ +\left[\left(\xi-m\right)\left(\beta+\frac{K_{s1}}{K_{b1}}\right)+\left(\beta+m\right)\left(\xi-\frac{K_{s1}}{K_{b1}}\right)+2\left(\frac{K_{s1}}{K_{b2}}\right)^2\right]\cosh\left(\sqrt{\xi}H\right)\cos\left(\sqrt{\beta}H\right)\end{array}\right\}=0, \tag{B1}$$

where:

$$m=\frac{K_{s1}K_{s2}-P\left(K_{s1}+K_{s2}\right)}{K_{b2}\left(K_{s2}-P\right)}. \tag{B2}$$

The solution to Eq. (B1) is obtained for:

$$\cos\left(\sqrt{\beta}H\right)=0\rightarrow\sqrt{\beta}H=\frac{\pi}{2}. \tag{B3}$$

Using Eqs. (34)–(36), the global critical buckling load P is obtained as:

$$P_{cr}=\frac{\pi^4K_{b1}K_{b2}K_{s2}+4H^2\pi^2K_{s1}K_{s2}\left(K_{b1}+K_{b2}\right)}{16H^4K_{s1}K_{s2}+4H^2\pi^2\left(K_{b1}K_{s1}+K_{b1}K_{s2}+K_{s1}K_{b2}\right)+\pi^4K_{b1}K_{b2}}. \tag{B4}$$

After some straightforward algebraic manipulations, the global critical buckling load P is obtained as:

$$P_{cr}=\left\{\left\{\left\{\left[\frac{\pi^2K_{b1}}{4H^2}\right]^{-1}+K_{s1}^{-1}\right\}^{-1}+\frac{\pi^2K_{b2}}{4H^2}\right\}^{-1}+K_{s2}^{-1}\right\}^{-1}. \tag{B5}$$

Since the load is applied vertically at the top of the structure, the global critical buckling load satisfies $q_{cr}=P_{cr}$, and therefore Eq. (B5) can be rewritten as:

$$q_{cr}=\left\{\left\{\left\{\left[\frac{\pi^2K_{b1}}{4H^2}\right]^{-1}+K_{s1}^{-1}\right\}^{-1}+\frac{\pi^2K_{b2}}{4H^2}\right\}^{-1}+K_{s2}^{-1}\right\}^{-1}. \tag{B6}$$